Original paper

Image analysis discloses differences in nuclear parameters between ERG+ and ERG– prostatic carcinomas

Krzysztof Okoń[1], Grzegorz Dyduch[1], Magdalena B. Białas[1], Katarzyna Milian-Ciesielska[1], Joanna Szpor[1], Iga Leszczyńska[1], Katarzyna Tyrak[2], Tomasz Szopiński[3], Piotr Chłosta[4]

[1]Department of Pathomorphology, Jagiellonian University Medical College, Krakow, Poland
[2]2nd Department of Internal Medicine after Professor Andrzej Szczeklik, Jagiellonian University Medical College, Krakow, Poland
[3]Mazovia Hospital, Warsaw, Poland
[4]Department of Urology, Jagiellonian University Medical College, Krakow, Poland

Prostatic carcinoma (PC) is the most frequent urologic cancer and one of the most frequent cancers in males; it is a heterogeneous disease, in terms of molecular features, morphology and prognosis. About half of cases depends on TMPRSS2-ETS translocation which leads to a production of ERG transcription factor. ERG+ and ERG– cancers seem to differ in a number of features, which could lead to an altered nuclear structure; the aim of the study was to test this hypothesis. The material consisted of total 39 PC cases, representing ERG+ and ERG–, as well as Gleason pattern 3 and 4. Filtering by color deconvolution and automatic segmentation were used, and the properly detected nuclei were manually selected. From each case fifty nuclei were obtained; then geometric features and texture parameters were assessed. The analysis of the collected data showed differences both between ERG+/ERG– and Gleason pattern 3 and 4 cases in most of the features analyzed. Our results suggest that indeed the ERG status, thus likely TMPRSS2-ETS translocation, has an impact on morphology of nuclei in PC, and their differences are evident enough to be detectable by image analysis.

Key words: male, neoplasm grading, TMPRSS2 protein, human, prostatic neoplasms, urologic neoplasms.

Introduction

Prostatic carcinoma (PC) is one of the most frequent tumors worldwide and in the Western world it is indeed the most common cancer in males and an important cause of death [1]. The most frequent genetic event in PC is a translocation involving ETS family genes, most often ERG; this results in ERG protein product overexpression [2], a feature present in about half of patients in Europe, including whose from our material [3]. The biologic and prognostic significance of ERG expression in PC remains unclear and is a subject of intense analysis.

The aim of the study was to collect a set of nuclear parameters, including both geometric and texture features, and to analyze them in relation to ERG expression. As it has been shown before that the PCs of different Gleason grade show differences in nuclear parameters [4, 5, 6, 7], we decided to compare lower- and higher-grade tumors. The preliminary version of the results was presented at 26th European Congress of Pathology [8].

Material and methods

The study material consisted of prostatectomy specimens from the files of Pathology Department. Immunohistochemistry for ERG was performed on tissue microarrays, as previously reported [3]. The cases were reevaluated and reclassified according to the current criteria [9, 10, 11]. From the obtained dataset four groups were established as a combination of the following features: lower-grade (Gleason pattern 3) or higher-grade (Gleason pattern 4) and ERG− or ERG+ (Fig. 1). The Table I shows the details of grading, however for making the analysis more evident, only Gleason pattern in the TMA core was used for analysis.

The images of hematoxylin-eosin stained tissue microarrays were taken on a Zeiss Axioscope microscope equipped with a $100\times$ oil immersion lens using a Nikon D5100 digital camera. Pictures (Fig. 2) were transferred to a personal computer, converted from Nikon raw image format into TIF format

Table I. Composition of experimental diets

Gleason score	N	%	ISUP grade	N	%
3 + 3 = 6	9	23.08	1	9	23.08
3 + 4 = 7	18	46.15	2	18	46.15
4 + 3 = 7	8	20.51	3	8	20.51
4 + 4 = 8	1	2.56	4	1	2.56
4 + 5 = 9	2	5.13	5	3	7.69
5 + 4 = 9	1	2.56			

and processed using color deconvolution algorithm. The resulting files were used for the segmentation of nuclei. The properly segmented nuclei were being selected by the operator until fifty nuclei were available for each case (Fig. 3). The images of the nuclei were then processed by a program which measured the geometric and textural features listed in Table II.
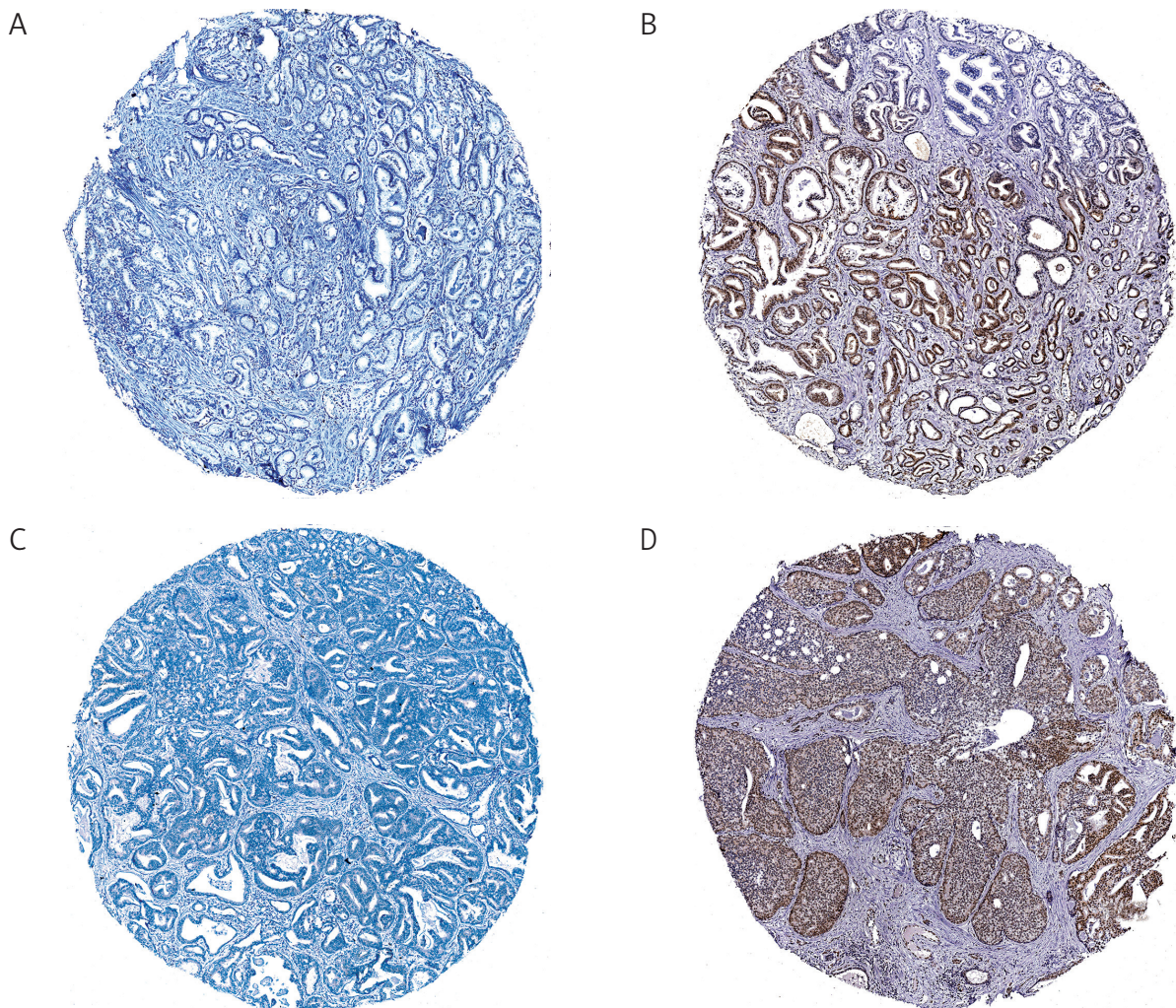

Fig. 1. Immunohistochemistry of the TMA tissue cores used for assessing ERG status; A) and B) are Gleason pattern 3; C) and D) are Gleason pattern 4; A) and C) are ERG−; B) and D) are ERG+; immunohistochemistry; magnification $0.3\times$
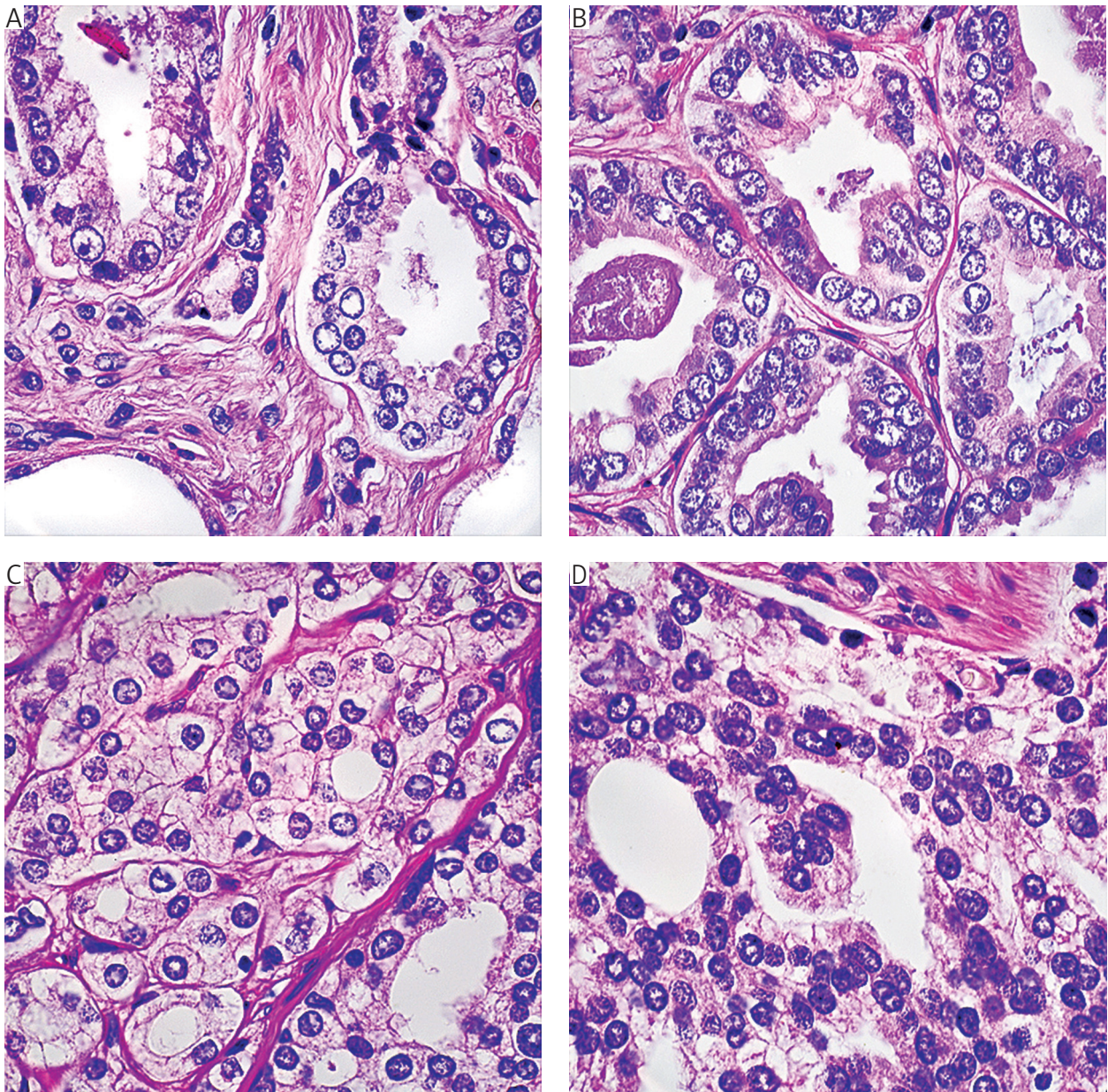
Fig. 2. Histology of prostatic carcinomas used in the study; A) and B) are Gleason pattern 3; C) and D) are Gleason pattern 4; A) and C) are ERG–; B) and D) are ERG+; hematoxylin and eosin; lens magnification 100×

Definitions of the form factors used:

$$SF = \frac{4\pi S}{L^2}$$

$$Rf = \frac{L_h}{L_v}$$

$$Rc = \frac{{}^2\sqrt{S/\pi}}{L/\pi}$$

$$compactnes = \frac{D_{min}}{D_{max}}$$

Where: L – nuclear perimeter, S – nuclear area, Lh – horizontal diameter, Lv – vertical diameter, D_{min} – minimum diameter, D_{max} – maximum diameter.

The image processing was performed with ImageJ 1.47V (National Institutes of Health), AnalySIS 3.2 (Soft Imaging Systems GmbH) software, color deconvolution macro (G. Landini, http://www.mecourse.com/landinig/) as well as macros developed by one of the authors (KO). Student's t test was used for comparison between groups. Interactions between factors was assessed using ANOVA. Significance level was set to 0.05. The data was analyzed using Statistica 12 (StatSoft, Tulsa CA, USA) and R package (R Foundation for Statistical Computing) [12].

Table II. Parameters used in the study (see [49, 50, 51] for details)

Simple geometric features
Area
Perimeter
Convex perimeter
Convex area
Equivalent circle diameter
Minimum, maximum and mean diameter

Form factors: SF, Rf, Rc, compactness

Texture features
Gray level correlation matrix derived (mean, SD, energy, contrast, homogeneity, entropy)
Central moments invariants ($\phi1$ to $\phi7$)
Gray level kurtosis
Gray level skewness

Results

The group under study consisted of 39 cases; the mean age of the patients was 62.58 (range 50 to 75 years, SD 5.89). The age of the patients did not show significant relationship with any of the analyzed variables. Eleven cases were pT2 (29.2%), 26 (66.7%) were pT3 and 2 (5.1%) were pT4. Details of grading are shown in Table I. For the study, areas with Gleason patter 3 or 4, either ERG+ or ERG− were selected. Among the four established study groups the following numbers were obtained: 9 cases of Gleason pattern 3, ERG− cancers; 11 cases of Gleason pattern 3, ERG+ cancers; 9 cases of Gleason pattern 4, ERG− cancers and 10 cases of Gleason pattern 4, ERG+ cancers. For each case at least fifty nuclei were measured. The results are shown in Table III. Individual case profiles are shown on Fig. 4, and the profiles averaged over the study group on Fig. 5. As might have been expected, the
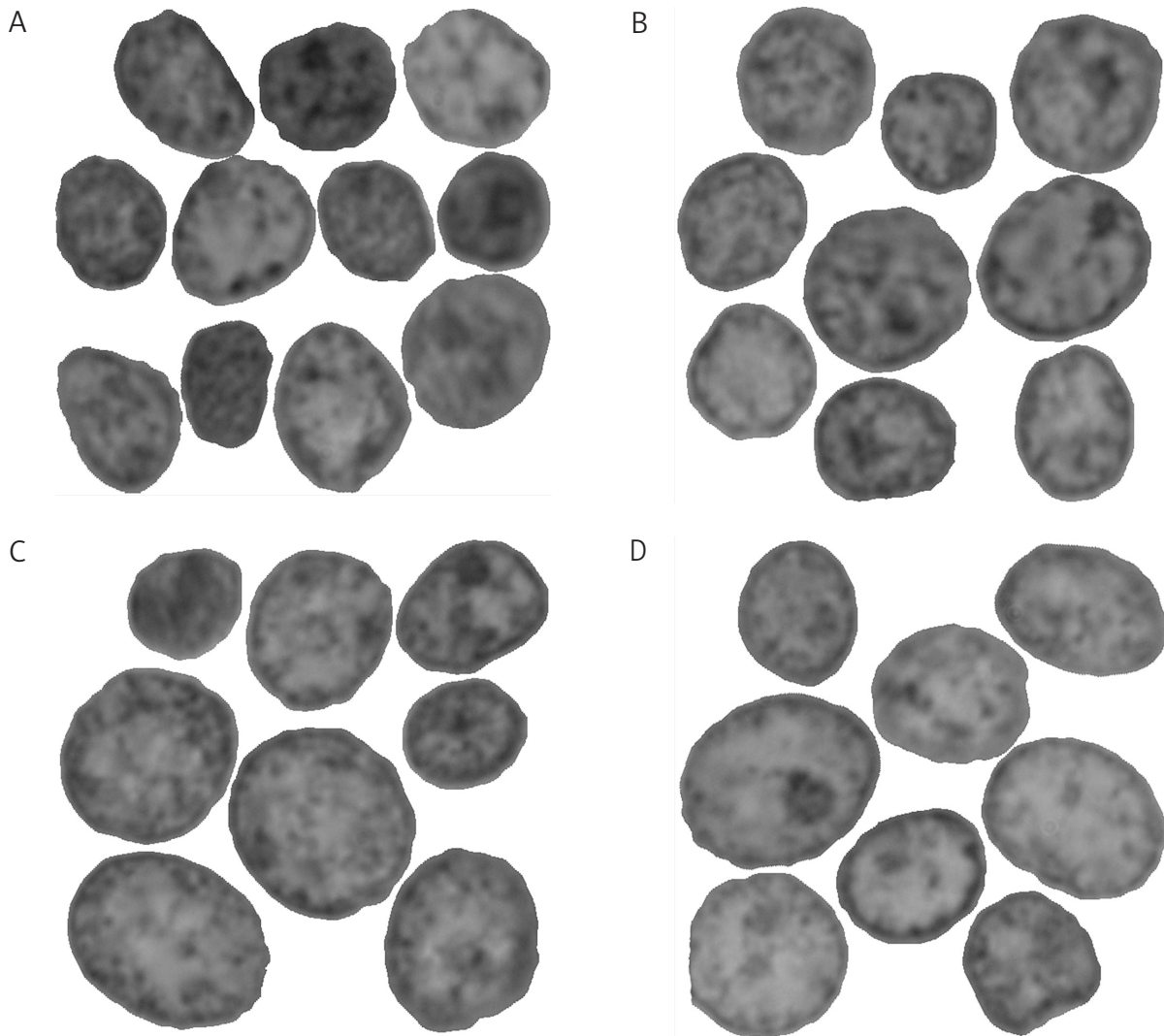

Fig. 3. Examples of individual segmented nuclei; A) and B) are Gleason pattern 3; C) and D are Gleason pattern 4; A) and C) are ERG−; B) and d are ERG+. Originals were in hematoxylin and eosin; lens magnification 100×

Table III. The descriptive statistics of the measured nuclear parameters

Parameter	Mean	Min.	Max.	SD
Area	47.894	17.234	117.981	15.844
Convex perimeter	26.186	16.047	46.348	4.220
Convex area	48.895	17.711	136.673	16.172
Equivalent circle diameter	7.710	4.684	12.256	1.239
Maximum diameter	8.840	5.273	15.551	1.511
Mean diameter	8.127	4.995	14.653	1.314
Minimum diameter	6.985	4.075	12.045	1.214
Perimeter	25.916	15.627	62.150	4.272
SF	0.875	0.348	0.960	0.044
Rf	1.006	0.508	2.159	0.187
Rc	0.468	0.295	0.490	0.012
Compact-ness	0.796	0.432	0.976	0.096
GV kurtosis	2051.805	114.967	68146.526	3183.838
GV skewness	195.148	23.874	2970.758	184.768
GLCM average	178.786	140.576	205.565	8.441
GLCM stdev	260.611	216.920	297.582	10.447
GLCM max	0.232	0.125	0.432	0.034
GLCM energy	0.114	0.033	0.591	0.048
GLCM contrast	353.797	151.334	684.435	88.212
GLCM homo-geneity	1.130	0.902	1.288	0.063
GLCM entropy	14.675	10.970	17.460	0.926
$\phi 1$	1.004	0.001	1.461	0.214
$\phi 2$	0.069	−2.682	3.701	0.964
$\phi 3$	7.231	0.000	192.203	12.477
$\phi 4$	7.684	0.000	168.287	11.749
$\phi 5$	−0.759	−400.845	2009.738	77.684
$\phi 6$	7.500	−76.007	573.799	31.675
$\phi 7$	−1.288	−1490.214	647.995	50.434

nuclei of Gleason pattern 4 cases were significantly larger and slightly more irregular than those of pattern 3 cases; there were also differences in the majority of textural features (Table IV). When analyzing the nuclei of ERG+ and ERG− cases it could be seen that in ERG+ cases they were significantly larger, yet they showed no difference in form factor values. However, there were differences in their textural parameters (Table V). Table VI shows comparison of unifactorial and multifactorial with interactions models.

Discussion

For some time now, it is known and accepted that a subset of PCs develop through a translocation involving ETS family genes and *TMPRSS2* gene [2, 13].

Under normal conditions, ETS family genes are expressed mainly by endothelial cells [14] and in translocation-related PC their genes comes under control of the androgen receptor. Androgen gene may be upregulated by the previous *NKX3.1* gene loss. This results in a significant expression of the transcription factors of the ETS family by the prostatic epithelial cells. Such carcinogenic mechanism is quite unusual for a carcinoma and similar to the phenomena which cause some mesenchymal or hematopoietic cancers [2, 13, 15]. Importantly, the expression of the ETS family transcription factors, ERG may be tested by immunohistochemistry and the results are highly correlated with the TMPRSS2-ETS translocation [13]. This offers an easy and cheap method for classifying PC genotype. Although a number of studies were published on the subject, it is still unclear
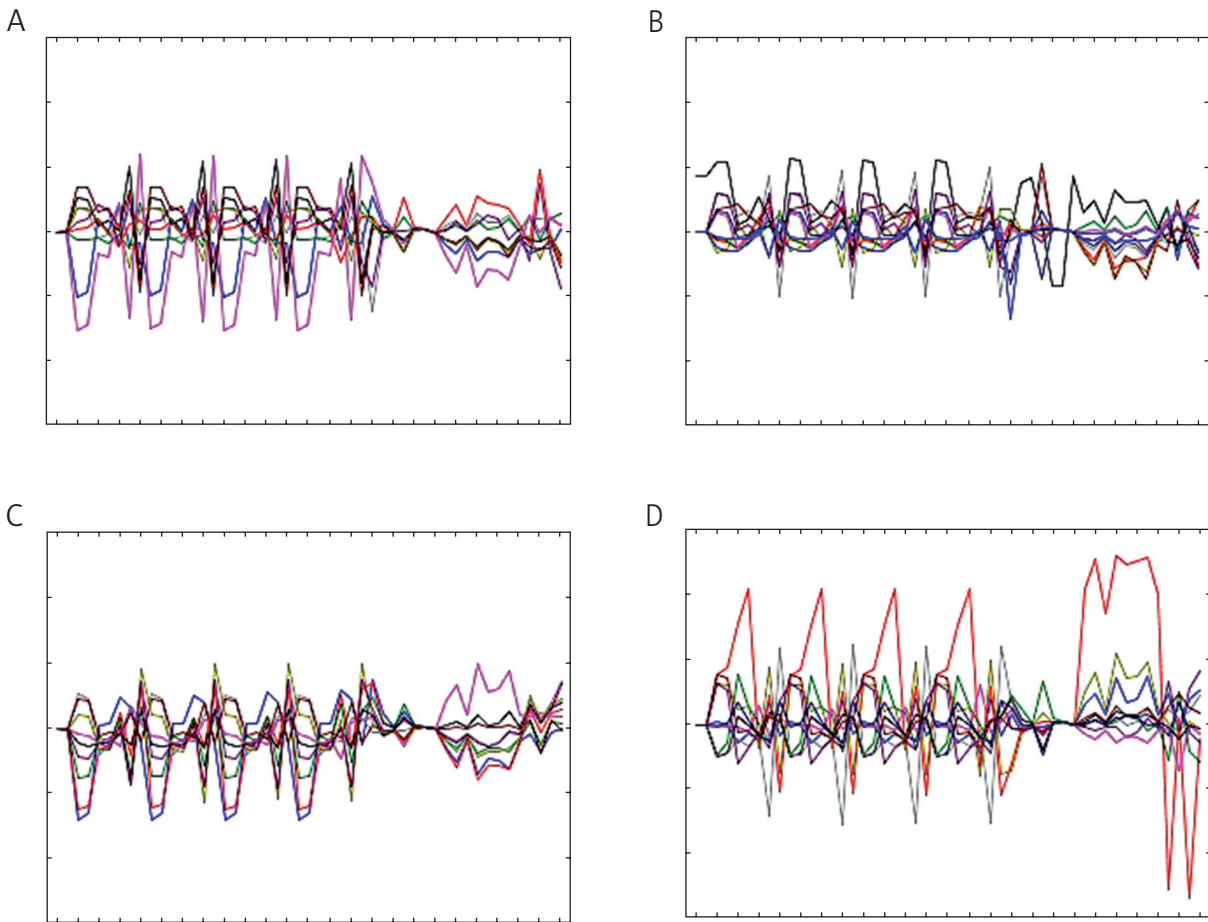
A

B

C

D

Fig. 4. Individual profiles of the cases under study; A) and B) are Gleason pattern 3; C) and D) are Gleason pattern 4; A) and C) are ERG−; B) and D) are ERG+; on the X axis the individual variables describing nuclear features are presented; on the Y axis their average values; for clarity, the names of the variables are omitted; all plots have the same scaling

whether translocation-associated prostate cancers are different in morphology or behavior [15]. In our opinion, some differences exist in terms of both morphology and stage as well as interaction with the tumor microenvironment [3, 16, 17, 18].

KDM1A, CHD1, and androgen receptor were identified as forming a complex responsible for targeted DNA breaks, which lead to TMPRSS2-ETS translocation [19]. TMPRSS2-ETS translocation may influence chromatin structure and stability by an upregulation of PIM1 kinase and a deregulation of Poly(ADP-Ribose) Polymerase [20, 21]. Another enzyme important for chromatin structure, which has been shown to participate in the generation of translocations in PC, is topoisomerase II beta. It is required for an expression of androgen-receptor regulated gene as well as it was shown to mediate double strand breaks of DNA in PC and in prostatic intraepithelial neoplasia (PIN) in an androgen receptor-mediated mechanism [22]. TMPRSS2-ETS translocation is the only one of the recurrent translocation – deletion events peculiar for PC. Another frequent alteration in PC is the 5q21 deletion. It has been shown that
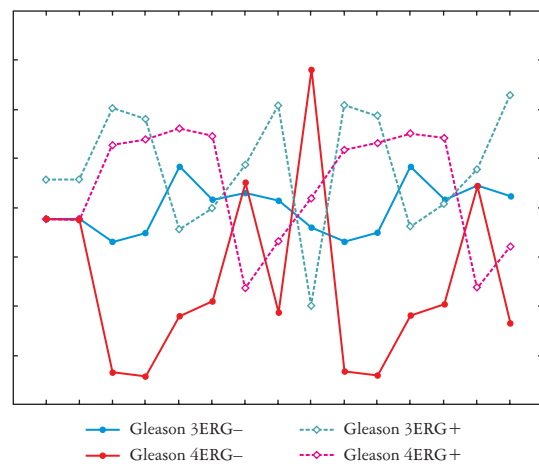
| Gleason 3ERG− | Gleason 3ERG+ |
| Gleason 4ERG− | Gleason 4ERG+ |

Fig. 5. Profiles of the study groups. On the X axis the individual variables describing nuclear features are presented; on the Y axis their average values; the variable names are omitted

it causes the loss of CHD1, which protein product – chromodomain helicase DNA binding protein 1, participates in chromatin remodeling. Interestingly, this

Table IV. The differences between pattern 3 and pattern 4 cases. For clarity, only means and significance levels for variables showing significant differences are shown (p – significance levels reached by Student t-test).

PARAMETER	PATTERN 3	PATTERN 4	P-VALUE
Area	45.343	50.671	< 0.001
Convex perimeter	26.186	26.831	< 0.001
Convex area	48.895	51.703	< 0.001
Equivalent circle diameter	7.511	7.927	< 0.001
Maximum diameter	8.709	8.983	< 0.001
Mean diameter	7.968	8.300	< 0.001
Minimum diameter	6.741	7.251	< 0.001
Perimeter	25.301	26.586	< 0.001
SF	0.871	0.881	< 0.001
Rc	0.466	0.469	< 0.001
GV kurtosis	0.780	0.813	< 0.001
GV skewness	2449.806	1618.661	< 0.001
GLCM average	221.115	166.887	< 0.001
GLCM stdev	179.698	177.794	< 0.001
GLCM max	261.736	259.386	< 0.001
GLCM energy	0.234	0.229	0.003
GLCM contrast	0.120	0.108	<0.001
GLCM homo-geneity	363.859	342.846	<0.001
GLCM entropy	1.140	1.120	<0.001
GV kurtosis	14.520	14.843	<0.001
$\phi 1$	0.975	1.037	<0.001
$\phi 3$	8.114	6.270	0.001
$\phi 6$	9.050	5.813	0.024

Table V. The differences between ERG– and ERG+ cases. For clarity, only means and significance levels for variables showing significant differences are shown (p – significance levels reached by Student t-test)

PARAMETER	ERG–	ERG+	P-VALUE
Area	45.597	49.904	< 0.001
Convex perimeter	25.582	26.714	< 0.001
Convex area	46.537	50.957	< 0.001
Equivalent circle diameter	7.536	7.863	< 0.001
Maximum diameter	8.638	9.017	< 0.001
Mean diameter	7.940	8.290	< 0.001
Minimum diameter	6.821	7.128	< 0.001
Perimeter	25.309	26.448	< 0.001
GLCM average	177.278	180.106	< 0.001
GLCM stdev	258.809	262.187	0.020
GLCM energy	0.111	0.116	< 0.001
GLCM contrast	368.024	341.350	<0.001
GLCM homo-geneity	1.125	1.135	<0.001
GLCM entropy	14.767	14.594	<0.001
$\phi 1$	1.028	0.983	<0.001
$\phi 3$	7.936	6.614	0.019
$\phi 4$	8.618	6.867	0.001

alteration is mutually exclusive with respect to TM-PRSS2-ETS translocation because the CHD1 protein product is required for the occurrence of this translocation [23, 24]. Altered expression of proteins acting on chromatin structure and the chromatin destabilization could result in a change of its structure visible at the microscopic level, similar to the one that may be noticed in other organs [24].

Image analysis is a powerful tool in histopathology. It may allow for a detection of differences between groups of cases which may be not evident visually. In the PC pathology the visual nuclear grading may fail [25] while image analysis may show significant results [4, 6, 7]. Currently this method is used for research purpose, although an implementation of the computer-aided diagnosis systems has been proposed [26]. Application of image analysis to histopathology is often difficult because of a large size and a complexity of the image, variability in staining as well as difficulty in segmentation [26]. Color de-

convolution is a relatively new tool in image analysis that has already gained a wide acceptance in quantitative pathology, as it allows an effective thresholding of histologic image [27, 28]. For the best of our knowledge, no publications concerning relationship between nuclear morphometry and ERG status in PC are available, although several studies on the application of image analysis in PC were published. Most of them concentrate on automatic cancer diagnosis or computer-aided grading.

Loeffler *et al.* [27] aimed to obtain a classification of PC on the same rules, but more objective than the standard Gleason method. Using two relatively simple parameters, they were able to classify the tumors into Gleason pattern 3 and Gleason pattern 4/5 with high accuracy. Venkataraman *et al.* [7] compared the features of Feulgen stained nuclei in Gleason pattern 4 PC. Although the aim of that study is very different from ours, they employed a similar analytical approach, using a large set of geometric and textural features on manually segmented nuclei. They found significant differences between tumors that were either Gleason 7 = 3 + 4 or 7 = 4 + 3. The later nuclei tended to be larger, more irregular and have coarser chromatin. That adds an argument to the separation of these categories, as seen in the new ISUP grading system [9]. Alexandratou *et al.* [29]

Table VI. Multifactorial analysis of interactions between ERG status and Gleason grade

PARAMETER	EFFECTS IN ADDITIVE MODEL		P-VALUE
	ERG−	ERG+	
Area	<< 0.001	<< 0.001	<< 0.001
Convex perimeter	<< 0.001	<< 0.001	<< 0.001
Convex area	<< 0.01	<< 0.01	< 0.01
Equivalent circle diameter	<< 0.001	<< 0.001	<< 0.001
Maximum diameter	<< 0.001	<< 0.001	<< 0.001
Mean diameter	<< 0.001	<< 0.001	<< 0.001
Minimum diameter	<< 0.001	<< 0.001	<< 0.001
Perimeter	<< 0.001	< 0.01	<< 0.001
GLCM average	<< 0.001	<< 0.001	< 0.05
GLCM stdev	<< 0.001	<< 0.001	< 0.01
GLCM energy	<< 0.001	NS	<< 0.001
GLCM contrast	< 0.01	< 0.05	<< 0.001
GLCM homo-geneity	<< 0.001	<< 0.001	NS
GLCM entropy	<< 0.001	<< 0.001	NS
φ1	<< 0.001	<< 0.001	NS

NS – non significant

used gray level correlation matrix method to emulate grading of PC by Gleason method. They achieved over 85% accuracy of the classification. In contrast to the present study, the analysis was applied to the overall image of the tumor without an extraction of the structures such as nuclei, cytoplasm or extracellular compartment. Veltri *et al.* group published a number of very interesting papers on quantitative methods in prostate cancer pathology [30, 31, 32, 33, 34, 35]. They used a Feulgen-stained tissue microarray and measured a large set of morphologic and textural features, similarly as in our study. These features were combining into 'quantitative nuclear grade'. They analyzed nuclear features of PC with different Gleason grades and compared them to normally appearing nuclei adjacent to the cancer [30]. Although some differences were seen between benign and malignant nuclei, as well as between PC with different grades, the features under study showed large overlap between the groups. Similar methodology was used to identify the cases with biochemical recurrence [36] with an accuracy exceeding this of combined stage and Gleason score, and also to predict survival in patients with biochemical recurrence [34]. These results were obtained using older staging and grading systems, and it would be interesting to see the influence of recent modifications of TNM and Gleason systems. Farjam *et al.* [37] tested the image analysis for diagnosis of PC achieved the accuracy exceeding 95%. In the segmented image they measured geometric features of the glands, Bektas *et al.* [38] compared the basic nuclear parameters in PC with different Gleason score. As could be expected, they showed an increase in nuclear size and irregularity with progression of the tumor grade.

Isharwal *et al.* [39] analyzed several morphometric features of the PC nuclei, including geometric and textural parameters, for determining the differences between organ-confined and advanced cancers. They found the ploidy status to be by far the most important difference. In multiparametric models, inclusion of ploidy status improved the model performance by 1.5% in relation to more traditional dataset. Waliszewski *et al.* proposed the use of fractal geometry to classify PCs as an alternative to Gleason score [40, 41, 42]. One of the interesting results was the difference between 3+4 and 4+3 cancer, a difference which is seen in other studies and emphasized by the new ISUP grading system [42, 43]. Huang *et al.* [44] also used fractal geometry for emulation PC classification by Gleason method. They achieved overall accuracy reaching 94.6%. It is also of important to note, that the previous classification system contained many poorly defined elements, extremely difficult to assess even by highly trained humans. Gertych *et al.* [28] analyzed PCs by machine learning approach. They used a set of descriptors to obtain classification of the image into stromal and epithelial compartments and then epithelial elements into benign and cancerous. The features used were related to gray level and the texture. Tabesh *et al.* [45, 46] used image analysis system of automatic diagnosis of PC as well as assessment of Gleason score. The accuracy of cancer diagnosis exceeded 95%, while accuracy of the classification into low and high grades exceeded 81%. They used features extracted from the color histograms, fractal dimensions and wavelets analysis combined with different classifiers, including Gaussian and KNN. Weyn *et al.* [47] analyzed chromatin structure in a set of normal and neoplastic precursor lesion from the colon, esophagus and prostate. A large set of features was normalized and grouped to form nuclear signatures used to compare different groups of cases. Prostate cases consisted of entirely normal glands, normal gland adjacent to carcinoma and PIN. They noticed significant differences between normal, low grade PIN and high grade PIN, but did not study PC cases.

DNA ploidy was analyzed by several authors. For example Lorenzato *et al.* [48] analyzed DNA ploidy Gleason 3 + 3 PC on core biopsy material. They found that clinically organ-confined cancers tended to be diploid significantly more frequently than the

advanced ones. This difference was more significant for tumors with low PSA level. In our material, the nuclei of Gleason 3 + 3 cases were slightly larger, but significant differences were seen in few textural features only (data not shown).

Conclusions

We have shown that the ERG+ and ERG– differ in their nuclear features. We hypothesize that this may be due to differences in their molecular pathogenesis, but this has to be clarified by further studies.

References

1. Siegel RL, Miller KD, Jemal A. Cancer statistics, 2016. CA Cancer J Clin 2016; 66: 7-30.
2. Tomlins SA, Rhodes DR, Perner S, et al. Recurrent fusion of TMPRSS2 and ETS transcription factor genes in prostate cancer. Science 2005; 310: 644-648.
3. Kaczmarczyk K, Dyduch G, Bialas M, et al. Frequency of ERG-positive prostate carcinoma in Poland. Pol J Pathol 2013; 64: 175-179.
4. Lin WC, Li CC, Epstein JI, et al. Curvelet-based texture classification of critical Gleason patterns of prostate histological images. In' 2016 IEEE 6th International Conference on Computational Advances in Bio and Medical Sciences. IEEE, New York 2016.
5. Rashid F, Ul Haque A. Frequencies of different nuclear morphological features in prostate adenocarcinoma. Ann Diagn Pathol 2011; 15: 414-421.
6. Ali S, Veltri R, Epstein JI, et al. Adaptive energy selective active contour with shape priors for nuclear segmentation and Gleason grading of prostate cancer. In: Medical image computing and computer-assisted intervention, Miccai 2011, Pt I. Fichtinger G, Martel A, Peters T (eds.). Springer-Verlag, Berlin 2011; 661.
7. Venkataraman G, Rycyna K, Rabanser A, et al. Morphometric signature differences in nuclei of Gleason pattern 4 areas in Gleason 7 prostate cancer with differing primary grades on needle biopsy. J Urol 2009; 181: 88-93.
8. Okon K, Dyduch G, Bialas M, et al. Nuclear parameters and ERG status in the carcinoma of the prostate. Virchows Arch 2014; 465: S163-S163.
9. Epstein JI, Egevad L, Amin MB, et al. The 2014 International Society of Urological Pathology (ISUP) consensus conference on Gleason grading of prostatic carcinoma: definition of grading patterns and proposal for a new grading system. Am J Surg Pathol 2015; 40: 244-252.
10. Humphrey PA, Moch H, Cubilla AL, et al. The 2016 WHO classification of tumours of the urinary system and male genital organs-Part B: prostate and bladder tumours. Eur Urol 2016; 70: 106-119.
11. Amin MB, Edge SB, Greene FL, et al. AJCC cancer staging manual: Springer International Publishing, 2017.
12. R Core Team: R: A Language and Environment for Statistical Computing. R Foundation for Statistical Computing, 2017.
13. Park K, Tomlins SA, Mudaliar KM, et al. Antibody-based detection of ERG rearrangement-positive prostate cancer. Neoplasia 2010; 12: 590-595.
14. Randi AM, Sperone A, Dryden NH, et al. Regulation of angiogenesis by ETS transcription factors. Biochem Soc Trans 2009; 37: 1248-1253.
15. Donovan MJ, Cordon-Cardo C. Predicting high-risk disease using tissue biomarkers. Curr Opin Urol 2013; 23: 245-251.
16. Strzepek A, Kaczmarczyk K, Bialas M, et al. ERG positive prostatic cancer may show a more angiogenetic phenotype. Pathol Res Pract 2014; 210: 897-900.
17. Milek K, Kaczmarczyk-Sekula K, Strzepek A, et al. Mast cells influence neoangiogenesis in prostatic cancer independently of ERG status. Pol J Pathol 2016; 67: 244-249.
18. Kaczmarczyk-Sekula K, Galazka K, Glajcar A, et al. Prostate cancer with different ERG status may show different FOXP3-positive cell numbers. Pol J Pathol 2016; 67: 313-317.
19. Metzger E, Willmann D, McMillan J, et al. Assembly of methylated KDM1A and CHD1 drives androgen receptor-dependent transcription and translocation. Nat Struct Mol Biol 2016; 23: 132-139.
20. Magistroni V, Mologni L, Sanselicio S, et al. ERG deregulation induces PIM1 over-expression and aneuploidy in prostate epithelial cells. PLoS One 2011; 6: e28162.
21. Brenner JC, Ateeq B, Li Y, et al. Mechanistic rationale for inhibition of Poly(ADP-Ribose) polymerase in ETS gene fusion-positive prostate cancer. Cancer Cell 2011; 19: 664-678.
22. Haffner MC, Aryee MJ, Toubaji A, et al. Androgen-induced TOP2B-mediated double-strand breaks and prostate cancer gene rearrangements. Nat Genet 2010; 42: 668-645.
23. Packer JR, Maitland NJ. The molecular and cellular origin of human prostate cancer. Biochim Biophys Acta Mol Cell Res 2016; 1863: 1238-1260.
24. Burkhardt L, Fuchs S, Krohn A, et al. CHD1 Is a 5q21 Tumor Suppressor Required for ERG Rearrangement in Prostate Cancer. Cancer Res 2013; 73: 2795-2805.
25. Wittschieber D, Kollermann J, Schlomm T, et al. Nuclear Grading Versus Gleason Grading in Small Samples Containing Prostate Cancer: A Tissue Microarray Study. Pathol Oncol Res 2010; 16: 479-484.
26. He L, Long LR, Antani S, et al. Histology image analysis for carcinoma detection and grading. Comput Methods Programs Biomed 2012; 107: 538-556.
27. Loeffler M, Greulich L, Scheibe P, et al. Classifying prostate cancer malignancy by quantitative histomorphometry. J Urol 2012; 187: 1867-1875.
28. Gertych A, Ing N, Ma Z, et al. Machine learning approaches to analyze histological images of tissues from radical prostatectomies. Comput Med Imaging Graph 2015; 46: 197-208.
29. Alexandratou E, Yova D, Gorpas D, et al. Texture analysis of tissues in Gleason grading of prostate cancer. In: Imaging, manipulation, and analysis of biomolecules, cells, and tissues VI. Farkas DL, Nicolau DV, Leif RC (eds.). SPIE – The International Society for Optical Engineering 2008; 85904-85904.
30. Veltri RW, Marlow C, Khan MA, et al. Significant variations in nuclear structure occur between and within Gleason grading patterns 3, 4, and 5 determined by digital image analysis. Prostate 2007; 67: 1202-1210.
31. Veltri RW, Miller MC, Partin AW, et al. Prediction of prostate carcinoma stage by quantitative biopsy pathology. Cancer 2001; 91: 2322-2328.
32. Veltri RW, Partin AW, Epstein JE, et al. Quantitative nuclear morphometry, Markovian texture descriptors, and DNA content captured on a CAS-200 Image analysis system, combined with PCNA and HER-2/neu immunohistochemistry for prediction of prostate cancer progression. J Cell Biochem Suppl 1994; 19: 249-258.

33. Veltri RW, Zhu G, Lee G, et al. Histomorphometry of digital pathology: case study in prostate cancer. Front Med Imaging 2014; 26: 301-326.

34. Khan MA, Walsh PC, Miller MC, et al. Quantitative alterations in nuclear structure predict prostate carcinoma distant metastasis and death in men with biochemical recurrence after radical prostatectomy. Cancer 2003; 98: 2583-2591.

35. Veltri RW, Isharwal S, Miller MC, et al. Long-term assessment of prostate cancer progression free survival: evaluation of pathological parameters, nuclear shape and molecular biomarkers of pathogenesis. Prostate 2008; 68: 1806-1815.

36. Veltri RW, Miller MC, Isharwal S, et al. Prediction of prostate-specific antigen recurrence in men with long-term follow-up postprostatectomy using quantitative nuclear morphometry. Cancer Epidemiol Biomarkers Prev 2008; 17: 102-110.

37. Farjam R, Soltanian-Zadeh H, Jafari-Khouzani K, et al. An image analysis approach for automatic malignancy determination of prostate pathological images. Cytometry Part B-Clinical Cytometry 2007; 72B: 227-240.

38. Bektas S, Bahadir B, Gun BD, et al. The relation between gleason score, and nuclear size and shape factors in prostatic adenocarcinoma. Turkish Journal of Medical Sciences 2009; 39: 381-387.

39. Isharwal S, Miller MC, Epstein JI, et al. DNA Ploidy as Surrogate for Biopsy Gleason Score for Preoperative Organ Versus Nonorgan-confined Prostate Cancer Prediction. Urology 2009; 73: 1092-1097.

40. Waliszewski P. The quantitative criteria based on the fractal dimensions, entropy, and lacunarity for the spatial distribution of cancer cell nuclei enable identification of low or high aggressive prostate carcinomas. Front Physiol 2016; 7: 16.

41. Waliszewski P, Wagenlehner F, Gattenlohner S, et al. Fractal geometry in the objective grading of prostate carcinoma. Urologe A 2014; 53: 1186-1194.

42. Waliszewski P, Wagenlehner F, Kribus S, et al. Objective grading of prostate carcinoma based on fractal dimensions. Gleason 3+4=7a not equal Gleason 4+3=7b. Urologe A 2014; 53: 1504-1511.

43. Epstein JI, Egevad L, Amin MB, et al. The 2014 International Society of Urological Pathology (ISUP) consensus conference on Gleason grading of prostatic carcinoma: definition of grading patterns and proposal for a new grading system. Am J Surg Pathol 2016; 40: 244-252.

44. Huang PW, Lee CH. automatic classification for pathological prostate images based on fractal analysis. IEEE Trans Med Imaging 2009; 28: 1037-1050.

45. Tabesh A, Teverovskiy M, Pang HY, et al. Multifeature prostate cancer diagnosis and Gleason grading of histological images. IEEE Trans Med Imaging 2007; 26: 1366-1378.

46. Tabesh A, Kumar VP, Pang HY, et al. Automated prostate cancer diagnosis and Gleason grading of tissue microarrays. In: Medical imaging 2005: image processing, Pt 1-3. Fitzpatrick JM, Reinhardt JM (eds.). Spie-Int Soc Optical Engineering, Bellingham 2005; 8-70.

47. Weyn B, Jacob W, da Silva VD, et al. Data representation and reduction for chromatin texture in nuclei from premalignant prostatic, esophageal, and colonic lesions. Cytometry 2000; 41: 133-138.

48. Lorenzato M, Rey D, Durlach A, et al. DNA image cytometry on biopsies can help the detection of localized Gleason 3+3 prostate cancers. J Urol 2004; 172: 1311-1313.

49. Okon K, Tomaszewska R, Nowak K, et al. Application of neural networks to the classification of pancreatic intraductal proliferative lesions. Anal Cell Pathol 2001; 23: 129-136.

50. Styczen M, Szpor J, Demczuk S, et al. Karyometric comparison of splenic and gastric marginal zone lymphomas. Anal Cell Pathol 2012; 35: 297-303.

51. Tomaszewska R, Okon K, Nowak K, et al. Proliferation index and karyometric features of pancreatic intraductal proliferative lesions. Anal Cell Pathol 1999; 19: 175-185.

Address for correspondence

Krzysztof Okoń
Department of Pathomorphology
Jagiellonian University Medical College
Grzegórzecka 16
31-531 Krakow, Poland
k.okon@uj.edu.pl